Lyapunov theory-based control strategy for multi-terminal MMC-HVDC systems

Reza Janbazi Ghadi, Majid Mehrasa, M. Ebrahim Adabi, Seddik Bacha

Lyapunov Theory-based Control Strategy for Multi-Terminal MMC-HVDC Systems

Reza Janbazi Ghadi[1], Majid Mehrasa[2*], Erfan Azimi[1], M. Ebrahim Adabi[3], Seddik Bacha[4]
1: Iranian Mines and Mining Industries Development and Renovation Organization (IMIDRO)
2: Dept. of Engineering and Architecture Universitá degli Studi di Trieste, Trieste, Italy
3: Intelligent Electrical Power Grids at Department of Electrical Sustainable Energy, Delft University of Technology, Delft, The Netherlands.
4: Univ. Grenoble Alpes, CNRS, Grenoble INP (Institute of Engineering Univ. Grenoble, Alpes), G2Elab, 38000 Grenoble, France

***Abstract*—** This paper presents a coordinated control strategy based on direct Lyapunov theory to handle the consistency of AC grids in a multi-terminal (MT) modular multilevel converter (MMC)-HVDC systems during varying both loads and DC link voltage. As the first contribution, a set of dynamic equations is proposed based on separating the dynamics of MMCs upper and lower arms state variables. The dynamics consists of only their related upper/lower arms state variables leading to more effective components for the steady state terms of proposed control technique. To develop the dynamic parts of the controller, the global asymptotical stability of MT MMC-HVDC system is assessed by direct Lyapunov method. As another advantage of the separated dynamic equations, the Lyapunov theory is able to exploit very simple decoupled components for the dynamic parts of proposed control functions. Moreover, in order to specify the variation trend of Lyapunov coefficients, further stability analysis contributes to demonstrating the effects of Lyapunov coefficients on the MMCs state variable errors and its dynamic. As another main contribution of this paper, two independent capability curves based on the power injection capability of the MMCs upper and lower arms, are obtained which will be assessed through changing the input and output voltages as well as MMC parameters. Finally, simulation results in MATLAB software are utilized to verify the validity of proposed control strategy.

***Index Terms*—** Multi-terminal HVDC, Modular multilevel converter, AC grid, Lyapunov theory, upper and lower arms, state variable error and its dynamic, independent capability curves.

I. NOMENCLATURES

Indices

k	*a,b,c*
n	*u,l*

Abbreviations

KVL	Kirchhoffs Voltage Law
AC	Alternating Current
DC	Direct Current
HVDC	High-Voltage Direct-Current
MMC	Modular Multilevel Converter
RERs	Renewable Energy Resources
VSCs	Voltage-Source Converters
MT MMC-HVDC	Multi-Terminal MMC-HVDC
SMs	Sub-Modules
MPPT	Maximum Power Point Tracking

Variables

i_{abc}	MMC output currents
i_{nk}	Currents of MMC's Upper and Lower Arms
$P_{n(dq)}$	Power of Upper and Lower Arms
i_{dc}	Current of DC-link of MMCs
i_{ndq}, i_{ndq}^*	Currents of MMC's Upper and Lower Arms in dq Reference Frame and its Reference Values
v_{dq}, v_{dq}^*	The output voltages of MMC in d-q Reference Frame and its Reference Values
v_k	Output voltages of MMC in a-b-c Reference Frame
v_{nk}	Modulation functions for upper and lower arms SMs of MMCs in abc reference frame
v_{ndq}, v_{ndq*}	Modulation Functions in dq Reference Frame and its Reference Values
$W(E)$	Lyapunov Energy Function
e	The Error of State Variables
v_{tdq}	Terminal Voltage of MMC
v_{dc}, v_{dc}^*	DC-link voltage and its Reference Value

Parameters

L,R	MMC Resistance and Inductance
L_n, R_n	Upper and Lower Arm Inductance and Resistance
$C_1=C_2=\ldots=C_n$	SMs Capacitor
ω	Angular Frequency of MMC Output Voltage
N	SMs Number in Each Arm
α_{ndq}	Lyapunov Coefficients of Dynamic Parts of Modulation Functions

II. INTRODUCTION

Power electronics converters (PECs) have always been considered as the vital materiel for integrating renewable energy resources (RERs) into power systems and also using RERs in autonomous electrical network structures [1-4]. Among PECs, Multi-level converters are regarded as the main alternative for RERs, which have been introduced as a proper solution to reduce harmonic content of output voltage in high power applications, to solve the issue of high power transfer, and also to improve the quality of the voltage with lower stress on the semiconductor switches [5-8]. Because of the features, these converters have been used in

many industrial applications such as DC network application [9], frequency control [10-11], STATCOM [12], HVDC [13], PV Panels MPPT [14] and so on.

Modular multilevel converters (MMCs) as one of the most effective multi-level PECs in power system applications, have been highly investigated in recent years, because MMC has several technical abilities at providing good performance in high voltage and power applications with high efficiency including modular structure, easy redundancy of SMs, decentralized energy storages, simple fault detection and clearance [15-20]. MMC which had been introduced by Marquardt and Lesnicar for the first time in 2003 [21], has been able to ease high voltage application with high power transfer in motor drive [22], HVDC system [23], static synchronous compensator [24], offshore DC wind turbine [25] and so on. Because of less loss and cost compared to AC transmission lines and also due to MMCs features, the importance of DC power transmission in the frame of MMC-based HVDC systems has become a priority for researchers to attain a stable operating condition for HVDC-connected electrical networks [26-28]. To this end, the challenges regarding the control system design for MMCs has been developed in these works [29-30]. The normalized DC-link voltage and the DC-link power variation have been the key factors for controlling the related active power set-point value of MMC station in Ref [31]. A fast model-based predictive control (FMPC) with low computational burden has been designed for grid-connected MMC in [32]. To reduce the computing time, the reference voltage vector among a large number of available multilevel voltage vectors in MMC could be found in a single step [32]. Optimal robust control design [33] and coordinated start-up control [34] have been performed to force MMC to reach smooth operation in HVDC system. In addition, the achieved control functions-based Lyapunov method has been combined with input-output feedback linearization technique to regulate the performance of MMC-based HVDC system under both load variations and fault condition [35].

Multi-Terminal (MT) MMC-based HVDC systems have been a developed next generation of HVDC-based systems which have several superiorities such as providing AC power grids with different frequencies, supplying much more distributed loads centers and injecting more active and reactive power [36-38]. As a power electronics-based power system, a complete control strategy should be designed for obtaining a proper MT HVDC system in presence of dynamical changes. To effectively damp the frequency fluctuations, a model predictive control with coordination capability has been designed for MT HVDC system in Ref [39]. In a meshed multi-terminal HVDC, a DC current flow control strategy has been proposed in Ref [40] to balance the DC branch currents. The power transmission in the HVDC system has

been aimed to reach its maximum value in Ref [41] by designing a voltage-current droop controller and keeping all voltages and currents of PECs within their design boundaries. Through the analysis of DC voltage, power deviation and droop coefficient, a droop control technique with tunable parameters has been designed to attain an optimized coordination control for a multi-terminal MMC-HVDC system connected to wind farms [42]. In addition to control design process, dynamical analysis and modelling challenge of MT HVDC system should be paid attention as well [43]. Ref [44] has showed that how the energy management strategies of the MMCs could impact on the dc voltage dynamics. Some of MT HVDC system can be made by a large diode rectifier-connected off-shore wind power plant. Ref [45] has focused on the detailed modeling and small-signal stability analysis of such HVDC system. The detailed dynamic model in [45] has been utilized for evaluating the system robustness against parametric uncertainties, communication delay and power level, in which the integration of the off-shore WPP into the on-shore electrical power system has also been guaranteed. Moreover, the modelling of HVDC system including hybrid breakers [46] and dynamic electro-magnetic-thermal modeling [47] have also been inquired.

Due to the nonlinearity features of dynamic models of MT MMC-HVDC systems, many nonlinear control strategies [48-53] can be proposed for accurate control of such systems. In this paper, a coordinated Lyapunov-based control strategy is designed for a MT MMC-HVDC system using a new set of dynamic equations. The proposed controller is aimed to provide stable frequency and voltage magnitude of AC grids in presence of both load and DC-link voltage fluctuations. The contributions of this manuscript can be explained as the follows, 1) As the first contribution, a separated dynamic model is proposed for MMCs in MT MMC-HVDC system. It means that the separated dynamic model consists of two sets of dynamic equations. The first set contains only the MMCs upper arm currents in d-q reference frame. Also, the second set is constituted from only the MMCs lower arm currents in d-q reference frame. This separated dynamic model is brought advantages leading to more effective components for the steady-state parts of proposed control technique. In addition, by using the new dynamic model, the Lyapunov-based dynamic components are involved with more effective terms to deal with the transient operating conditions of MMCs in MT MMC-based HVDC system, 2) For the first time, as the second contributions of this manuscript, two capability curves are proposed based on the power injection capability within the upper and lower arms of MMCs. These curves are derived using the separated dynamics of MMCs. The operating area variations of these curves are assessed under steady state condition, the increment of the input and output voltages of MMCs, the increment of MMCs resistance, the

increment of MMCs inductance and also the negative and positive values of dilu/dt. These curves can highly contribute to accurate performance of coordination abilities of proposed control strategies, and 3) As the third contribution of this manuscript, a new method based on evaluating three-dimension curves are presented in this manuscript to figure out the appropriate trend of Lyapunov coefficients changes. To this end, several authentic mathematical relations between the Lyapunov coefficients and MMCs state variables errors are obtained. Through the evaluation of the curves which are plotted by the relations, the appropriate variation trend can be driven for the Lyapunov coefficients based on minimizing the MMCs state variables errors. The various sections of the paper are organized as the following. Two fist sections are included nomenclatures and introduction. Section III presents the description of the considered MT MMC-HVDC system in which the proposed dynamic equations are presented in this section as well. Section IV, sub-section A focuses on the dynamic part design of proposed control strategy. In next sub-section, Lyapunov coefficient effects on MMC error dynamics are assessed. Two independent capability curves are presented in Section V. Simulations results and conclusion are discussed in sections VI and VII, respectively.

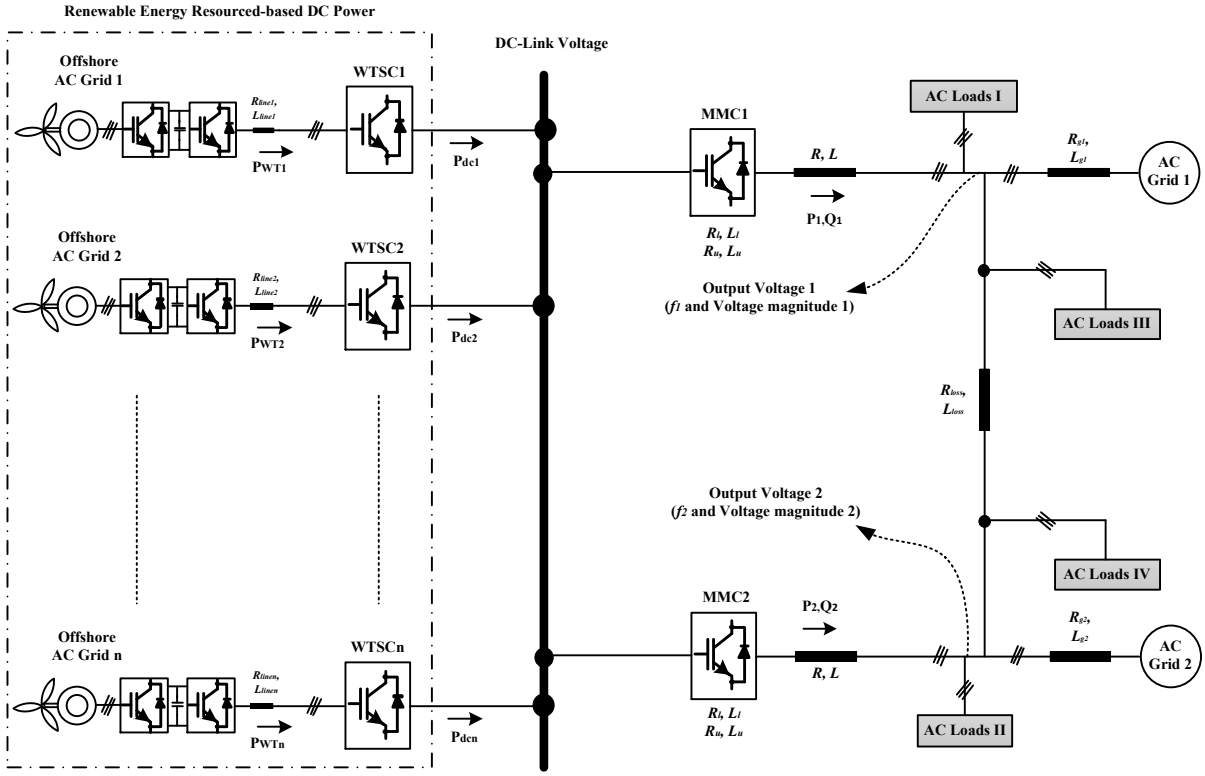

(a)

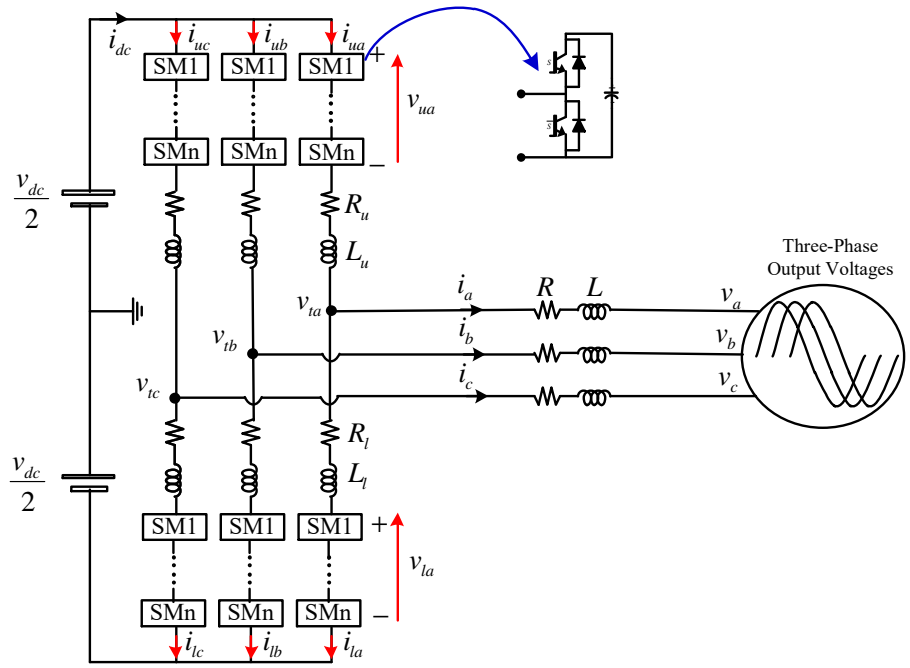

(b)

Fig. 1. The Multi-terminal MMC-based HVDC studied in this paper.

III. The Multi-Terminal MMC-HVDC System Description

This paper investigates the MT MMC-HVDC system shown in Fig. 1(a). According to this figure, two MMCs with both resistance and inductance in each arm and its output are connected to two AC grids. Two loads are considered in each power grid. In order to assay the dynamic performance of the MT MMC-HVDC system, several loads are linked to the common line between the two AC grids. The DC-link voltage of this system is supplied through RERs-based power converters. It is assumed that the DC-link voltage can be fluctuated through these converters. The detailed configuration of MMCs is illustrated in Fig. 1(b).

A. Proposed Dynamics Model

Two MMCs in Fig. 1(a) will utilize the same structure exhibited in Fig. 1(b). Thus, the achieved dynamic model in this section will be employed for both MMCs at the same time. By applying KVL's law from DC-link to output side of MMCs, the following dynamic models are driven,

$$v_k + L\frac{di_k}{dt} + Ri_k + L_u\frac{di_{uk}}{dt} + R_u i_{uk} - \frac{v_{dc}}{2} + v_{uk} = 0 \tag{1}$$

$$-v_k - L\frac{di_k}{dt} - Ri_k + L_l\frac{di_{lk}}{dt} + R_l i_{lk} - \frac{v_{dc}}{2} + v_{lk} = 0 \tag{2}$$

As it was mentioned in the Nomenclatures section, "*k*" demonstrates the abbreviation

statements of three phases that are "*a*", "*b*" and "*c*", respectively. The relationship between the MMCs arms and output currents can meet,

$$i_k = i_{uk} - i_{lk} \tag{3}$$

The relation (3) is substituted into (1) and (2) leading to the dynamic equations (4) and (5), respectively. In these equations, except for v_k and v_{dc}, the remained state variables are the currents and voltages of the MMCs upper and lower arms according to,

$$v_k + L\frac{di_{uk}}{dt} - L\frac{di_{lk}}{dt} + Ri_{uk} - Ri_{lk} + L_u\frac{di_{uk}}{dt} + R_u i_{uk} - \frac{v_{dc}}{2} + v_{uk} = 0 \tag{4}$$

$$v_k + L\frac{di_{uk}}{dt} - L\frac{di_{lk}}{dt} + Ri_{uk} - Ri_{lk} - L_l\frac{di_{lk}}{dt} - R_l i_{lk} + \frac{v_{dc}}{2} - v_{lk} = 0 \tag{5}$$

By summing up (4) and (5) and after some mathematical simplifications, the following dynamic equations are obtained,

$$\left(2L + L_u\right)\frac{di_{uk}}{dt} + \left(2R + R_u\right)i_{uk} + v_{uk} + v_k = 0 \tag{6}$$

$$\left(2L + L_l\right)\frac{di_{lk}}{dt} + \left(2R + R_l\right)i_{lk} + v_{lk} - v_k = 0 \tag{7}$$

The proposed dynamic equations can be achieved according to (6) and (7). The extended terms of (6) and (7) are given in Annex A. Except for v_k, it can be realized that the equations (6) and (7) consists of only upper and lower state variables, respectively. These feature will contribute to more effective components for steady-state and dynamic parts of proposed control technique. To further dynamical analysis, the MMCs arms currents which pass through the SMs capacitors will be taken into account as well. Fig. 1(b) is used to write the relations between the modulation functions and arms currents as the follows,

$$\frac{C}{N}\frac{dv_{uk}}{dt} = i_{uk} \tag{8}$$

$$\frac{C}{N}\frac{dv_{lk}}{dt} = i_{lk} \tag{9}$$

In this paper, it is aimed to execute the control design process in d-q reference frame. For this reason, the park transformation matrix in annex B can be used. The proposed dynamic model in dq reference frame will be obtained by applying the inversed matrix (10) to (6)-(9),

$$\begin{bmatrix} x_a \\ x_b \\ x_c \end{bmatrix} = \frac{3}{2}\begin{bmatrix} \cos(\theta) & \cos\left(\theta-\frac{2\pi}{3}\right) & \cos\left(\theta+\frac{2\pi}{3}\right) \\ \sin(\theta) & \sin\left(\theta-\frac{2\pi}{3}\right) & \sin\left(\theta+\frac{2\pi}{3}\right) \\ \frac{1}{2} & \frac{1}{2} & \frac{1}{2} \end{bmatrix}^{-1} \begin{bmatrix} x_d \\ x_q \\ x_0 \end{bmatrix} \tag{10}$$

Where $\theta=\omega t$. The angular frequency ω is calculated based on substituting the desired value of frequency into ω leading to $\theta=2\pi f^{*}t$. As a consequence, the matrix representation-based dynamic model of the multi-terminal MMC-based HVDC system can meet,

$$\frac{d}{dt}\begin{bmatrix} i_{nd} \\ i_{nq} \end{bmatrix} = \begin{bmatrix} -\frac{(2R+R_n)}{(2L+L_n)} & +\omega \\ -\omega & -\frac{(2R+R_n)}{(2L+L_n)} \end{bmatrix}\begin{bmatrix} i_{nd} \\ i_{nq} \end{bmatrix} - \frac{1}{(2L+L_n)}\begin{bmatrix} v_{nd} \\ v_{nq} \end{bmatrix} \mp \frac{1}{(2L+L_n)}\begin{bmatrix} v_d \\ v_q \end{bmatrix} \tag{11}$$

$$\frac{d}{dt}\begin{bmatrix} v_{nd} \\ v_{nq} \end{bmatrix} = \begin{bmatrix} 0 & \omega \\ -\omega & 0 \end{bmatrix}\begin{bmatrix} v_{nd} \\ v_{nq} \end{bmatrix} + \frac{N}{C}\begin{bmatrix} i_{nd} \\ i_{nq} \end{bmatrix} \tag{12}$$

As it was already mentioned in Nomenclature, the indices "*n*" has pointed out the abbreviation of upper and lower terms that are "*u*" and "*l*", respectively. In addition, in (11), the sign of "-" and "+" are belong to the state variables regarding the upper and lower arms of MMCs, respectively.

B. Steady-State Parts with Error-based Dynamic Model of Proposed Control Technique

The proposed control strategy will possess two steady-state and dynamic parts. The dynamic parts will be involved with the errors of all state variables of MT MMC-HVDC system presented in (13),

$$E = \begin{bmatrix} e_{iud} = i_{ud} - i_{ud}^{*} \\ e_{iuq} = i_{uq} - i_{uq}^{*} \\ e_{ild} = i_{ld} - i_{ld}^{*} \\ e_{ilq} = i_{lq} - i_{lq}^{*} \\ e_{vud} = v_{ud} - v_{ud}^{*} \\ e_{vuq} = v_{uq} - v_{uq}^{*} \\ e_{vld} = v_{ld} - v_{ld}^{*} \\ e_{vlq} = v_{lq} - v_{lq}^{*} \end{bmatrix} \tag{13}$$

In addition, the errors of d and q components of modulation functions and MMCs output voltages are defined as $e_{vud(q)}=v_{ud(q)}-v^{*}_{ud(q)}$, $e_{vld(q)}=v_{ld(q)}-v^{*}_{ld(q)}$, and $e_{vd(q)}=v_{d(q)}-v^{*}_{d(q)}$. The dynamic parts of proposed control technique will be analyzed in section IV. But, the steady-state components of proposed control strategy can be archived when all defined errors are

equalized to zero. In this condition, by substituting the reference values of MMCs state variables into (11), the steady-state parts of proposed modulation functions can meet,

$$v_{ud}^{*}=-\left(2L+L_u\right)\frac{di_{ud}^{*}}{dt}-\left(2R+R_u\right)i_{ud}^{*}+\omega\left(2L+L_u\right)i_{uq}^{*}-v_d^{*} \tag{14-a}$$

$$v_{uq}^{*}=-\left(2L+L_u\right)\frac{di_{uq}^{*}}{dt}-\left(2R+R_u\right)i_{uq}^{*}-\omega\left(2L+L_u\right)i_{ud}^{*}-v_q^{*} \tag{14-b}$$

$$v_{ld}^{*}=-\left(2L+L_l\right)\frac{di_{ld}^{*}}{dt}-\left(2R+R_l\right)i_{ld}^{*}+\omega\left(2L+L_l\right)i_{lq}^{*}+v_d^{*} \tag{14-c}$$

$$v_{lq}^{*}=-\left(2L+L_l\right)\frac{di_{lq}^{*}}{dt}-\left(2R+R_l\right)i_{lq}^{*}-\omega\left(2L+L_l\right)i_{ld}^{*}+v_q^{*} \tag{14-d}$$

As it can be understood from (14-a)-(14-d), all terms consist of only steady-state values of the MT MMC-HVDC system state variables as well as the system parameters. The error-based dynamic model of MMCs arms currents is achieved through subtracting (11) from (14) according to,

$$\frac{d}{dt}\begin{bmatrix}e_{ind}\\e_{inq}\end{bmatrix}=\begin{bmatrix}-\dfrac{\left(2R+R_n\right)}{\left(2L+L_n\right)} & +\omega\\ -\omega & -\dfrac{\left(2R+R_n\right)}{\left(2L+L_n\right)}\end{bmatrix}\begin{bmatrix}e_{ind}\\e_{inq}\end{bmatrix}-\frac{1}{\left(2L+L_n\right)}\begin{bmatrix}e_{vnd}\\e_{vnq}\end{bmatrix}\mp\frac{1}{\left(2L+L_n\right)}\begin{bmatrix}e_{vd}\\e_{vq}\end{bmatrix} \tag{15}$$

The dynamic model (12) is written in its steady-state condition according to,

$$\frac{d}{dt}\begin{bmatrix}v_{nd}^{*}\\v_{nq}^{*}\end{bmatrix}=\begin{bmatrix}0 & \omega\\ -\omega & 0\end{bmatrix}\begin{bmatrix}v_{nd}^{*}\\v_{nq}^{*}\end{bmatrix}+\frac{N}{C}\begin{bmatrix}i_{nd}^{*}\\i_{nq}^{*}\end{bmatrix} \tag{16}$$

As a consequence, the error-based dynamic model of modulation functions is achieved through subtracting (12) from (16),

$$\frac{d}{dt}\begin{bmatrix}e_{vnd}\\e_{vnq}\end{bmatrix}=\begin{bmatrix}0 & \omega\\ -\omega & 0\end{bmatrix}\begin{bmatrix}e_{vnd}\\e_{vnq}\end{bmatrix}+\frac{N}{C}\begin{bmatrix}e_{ind}\\e_{inq}\end{bmatrix} \tag{17}$$

The error dynamic models of MMCs in (15) and (17) will be employed for designing direct Lyapunov method-based control strategy.

IV. THE DYNAMIC PART OF PROPOSED CONTROL STRATEGY

A. Direct Lyapunov Method (DLM)

Direct Lyapunov method is utilized in this sub-section to achieve the transient components of proposed control technique. To this end, an energy function should be defined to satisfy the conditions given in (18),

$$W(0)=0 \quad (18)$$
$$W(\tilde{e})>0 \quad \forall\ \tilde{e}\neq 0$$
$$W(\tilde{e})\to\infty \ \ as\ \ \|\tilde{e}\|\to\infty$$
$$\dot{W}(\tilde{e})<0 \quad \forall\ \tilde{e}\neq 0$$

Lyapunov theory tends to provide global stable margin for MT MMC-HVDC system through controlling the state variables of the energy storage elements. For this reason, the following Lyapunov energy function will be defined for the MT MMC-HVDC system under study,

$$W(\tilde{e})=0.5(2L+L_u)e_{iud}^2+0.5(2L+L_u)e_{iuq}^2+0.5(2L+L_l)e_{ild}^2+0.5(2L+L_l)e_{ilq}^2 \quad (19)$$
$$+0.5Ce_{vud}^2+0.5Ce_{vuq}^2+0.5Ce_{vld}^2+0.5Ce_{vlq}^2$$

Another reason for constructing the energy function based on the errors of MMCs state variables is to achieve the dynamic parts of proposed control strategy based on direct Lyapunov method. In fact, using the direct Lyapunov method, it is guaranteed that the error dynamics of MMCs can lead to asymptotical global stability for the MT MMC-HVDC system. Based on (18), the derivative of (19) should be obtained,

$$\frac{dW(\tilde{e})}{dt}=(2L+L_u)e_{iud}\frac{de_{iud}}{dt}+(2L+L_u)e_{iuq}\frac{de_{iuq}}{dt}+(2L+L_l)e_{ild}\frac{de_{ild}}{dt}+(2L+L_l)e_{ilq}\frac{de_{ilq}}{dt} \quad (20)$$
$$+Ce_{vud}\frac{de_{vud}}{dt}+Ce_{vuq}\frac{de_{vuq}}{dt}+Ce_{vld}\frac{de_{vld}}{dt}+Ce_{vlq}\frac{de_{vlq}}{dt}$$

As it can be seen from (20), the errors and the errors dynamics are appeared in Lyapunov function derivative. Using (15) and (17), each term of the Lyapunov function derivative can be obtained as the follows,

$$\begin{cases}\dfrac{de_{ind}}{dt}e_{ind}=-\dfrac{(2R+R_n)}{(2L+L_n)}e_{ind}^2+\omega e_{inq}e_{ind}-\dfrac{1}{(2L+L_n)}e_{vnd}e_{ind}\mp\dfrac{1}{(2L+L_n)}e_{vd}e_{ind}\\ \dfrac{de_{inq}}{dt}e_{inq}=-\dfrac{(2R+R_n)}{(2L+L_n)}e_{inq}^2-\omega e_{ind}e_{inq}-\dfrac{1}{(2L+L_n)}e_{vnq}e_{inq}\mp\dfrac{1}{(2L+L_n)}e_{vq}e_{inq}\end{cases} \quad (21)$$

$$\begin{cases}\dfrac{de_{vnd}}{dt}e_{vnd}=\omega e_{vnq}e_{vnd}+\dfrac{N}{C}e_{ind}e_{vnd}\\ \dfrac{de_{vnq}}{dt}e_{vnq}=-\omega e_{vnd}e_{vnq}+\dfrac{N}{C}e_{inq}e_{vnq}\end{cases} \quad (22)$$

In order to simplify (15) as much as possible, the relations (21) and (22) will be substituted into (20) leading to the equation (28),

$$\frac{dW(\tilde{e})}{dt} = -(2R+R_u)e^2_{iud} - (2R+R_u)e^2_{iuq} - (2R+R_l)e^2_{ild} - (2R+R_l)e^2_{ilq} \quad (23)$$
$$+(-e_{vud} + Ne_{vud} - e_{vd})e_{iud}$$
$$+(-e_{vuq} + Ne_{vuq} - e_{vq})e_{iuq}$$
$$+(-e_{vld} + Ne_{vld} + e_{vd})e_{ild}$$
$$+(-e_{vlq} + Ne_{vlq} + e_{vq})e_{ilq}$$

In order to reach a global stable MT MMC-HVDC system, the derivative of Lyapunov function in (23) must be negative. It is obvious from (23) that the terms multiplied by the system resistances are always negative. It means that,

$$-(2R+R_u)e^2_{iud} < 0 \quad (24)$$
$$-(2R+R_u)e^2_{iuq} < 0$$
$$-(2R+R_l)e^2_{ild} < 0$$
$$-(2R+R_l)e^2_{ilq} < 0$$

The inequalities (23) will be true when $e_{ind} \neq 0$ and $e_{ind} \neq 0$. In order to reach negative value for (23) in all operating conditions, other terms (23) should be supposed as the following,

$$(-e_{vud} + Ne_{vud} - e_{vd}) = \alpha_{ud(q)}e_{iud} \quad (25)$$
$$(-e_{vuq} + Ne_{vuq} - e_{vq}) = \alpha_{ud(q)}e_{iuq}$$
$$(-e_{vld} + Ne_{vld} + e_{vd}) = \alpha_{ud(q)}e_{ild}$$
$$(-e_{vlq} + Ne_{vlq} + e_{vq}) = \alpha_{ud(q)}e_{ilq}$$

Where $\alpha_{ud(q)}$ and $\alpha_{ld(q)}$ are Lyapunov coefficients that should be negative. By rearranging the terms in (25), the dynamic parts of proposed modulation functions can meet,

$$e_{vud(q)} = \frac{\alpha_{ud(q)}e_{iud(q)} + e_{vd(q)}}{N-1} \quad (26)$$

$$e_{vld(q)} = \frac{\alpha_{ld(q)}e_{ild(q)} - e_{vd(q)}}{N-1} \quad (27)$$

It should be noticed that the Lyapunov coefficients of $\alpha_{ud(q)}$ and $\alpha_{ld(q)}$ have the Ohm dimension in which it leads to the same Volt dimension for both sides of (26) and (27). Also, as it is known, “N” has no dimension. It can be realized from (26) and (27) that the dynamics parts of proposed upper and lower modulation functions are accurately dependent on their proportional current errors as well as the MMCs output voltages. The detailed schematic of proposed control technique is illustrated in Fig.2. According to this figure, the proposed modulation function of each arm is proportional to its related MMCs arms current and voltage. This point contributes to the decoupling feature enhancement of proposed control strategy under various operating conditions. Level-Shifted Pulse-Width Modulation

(LSPWM) is used for the proposed modulation functions as well. On the other hand, the stead-state components of proposed control technique in Fig. 2 will be obtained using (14-a) to (14-d).

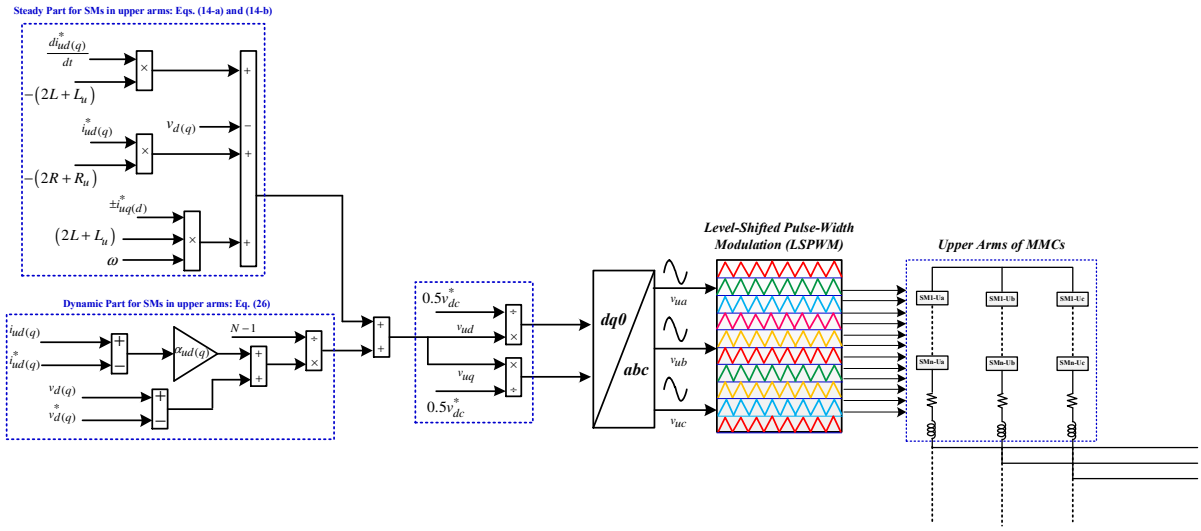

(a)

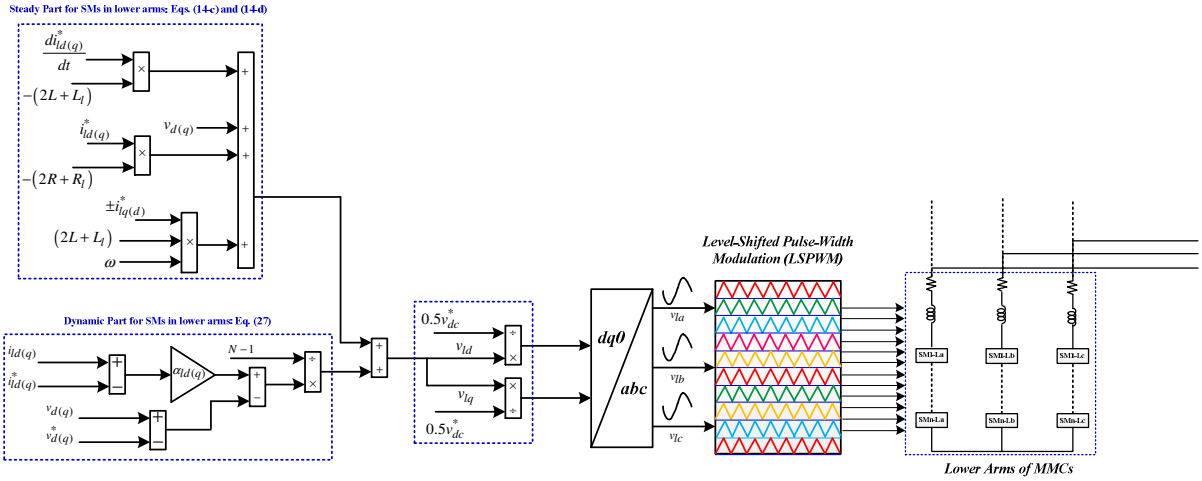

(b)

Fig.2. The proposed control strategy for each arm of MMCs used in multi-terminal HVDC system. The proposed control technique for (a) SMs switches in upper arms, and (b) SMs switches in lower arms.

B. Lyapunov Coefficient Effects on MMCs Error Dynamics

Proposed control technique based on Lyapunov method has several coefficients that will impact on the errors of MMCs state variables and its dynamics as well. To evaluate the effects of these coefficients, the relations between the Lyapunov coefficients and MMC errors must be firstly driven. To this end, relations (21), (26) and (27) are used to meet the following differential equations,

$$\begin{cases} \dfrac{de_{iud}}{dt} = -\dfrac{(2R+R_u)}{(2L+L_u)}e_{iud} + \omega e_{iuq} - \dfrac{1}{(2L+L_u)}\left[\dfrac{\alpha_{ud}e_{iud}+e_{vd}}{N-1}\right] - \dfrac{1}{(2L+L_u)}e_{vd} \\ \dfrac{de_{ild}}{dt} = -\dfrac{(2R+R_l)}{(2L+L_l)}e_{ild} + \omega e_{ilq} - \dfrac{1}{(2L+L_l)}\left[\dfrac{\alpha_{ld}e_{ild}-e_{vd}}{N-1}\right] + \dfrac{1}{(2L+L_l)}e_{vd} \end{cases} \quad (28)$$

The relation (28) will be rearranged based on MMCs state variable errors. After some mathematical manipulations, the d-component of MMCs state variable errors for upper and lower arms can be achieved according to (29) and (30), respectively,

$$e_{iud} = \frac{-\dfrac{de_{iud}}{dt} - \dfrac{1}{(2L+L_u)}\left(\left[\dfrac{1}{N-1}\right]+1\right)e_{vd} + \omega e_{iuq}}{\dfrac{1}{(2L+L_u)}\left((2R+R_u)+\left[\dfrac{\alpha_{ud}}{N-1}\right]\right)} \quad (29)$$

$$e_{ild} = \frac{-\dfrac{de_{ild}}{dt} + \dfrac{1}{(2L+L_l)}\left(\left[\dfrac{1}{N-1}\right]+1\right)e_{vd} + \omega e_{ilq}}{\dfrac{1}{(2L+L_l)}\left((2R+R_l)+\left[\dfrac{\alpha_{ld}}{N-1}\right]\right)} \quad (30)$$

The three-dimension curves based on relation (29) are plotted according to Fig. 3(a) and (b). As it can be realized from Fig. 3(a), when the current error of e_{iuq} is increased, the current error e_{iud} and its dynamic de_{iud}/dt will be noticeably increased as well. In this condition, the positive values for Lyapunov coefficients can contribute to the reduction of both e_{iud} and de_{iud}/dt as depicted in Fig. 3(a). Moreover, Fig. 3(b) illustrates that the larger interval for the Lyapunov coefficients can lead to achieving smaller values for the current error and its dynamic when the error e_{iuq} is changed. The same outcomes can be achieved for (30).

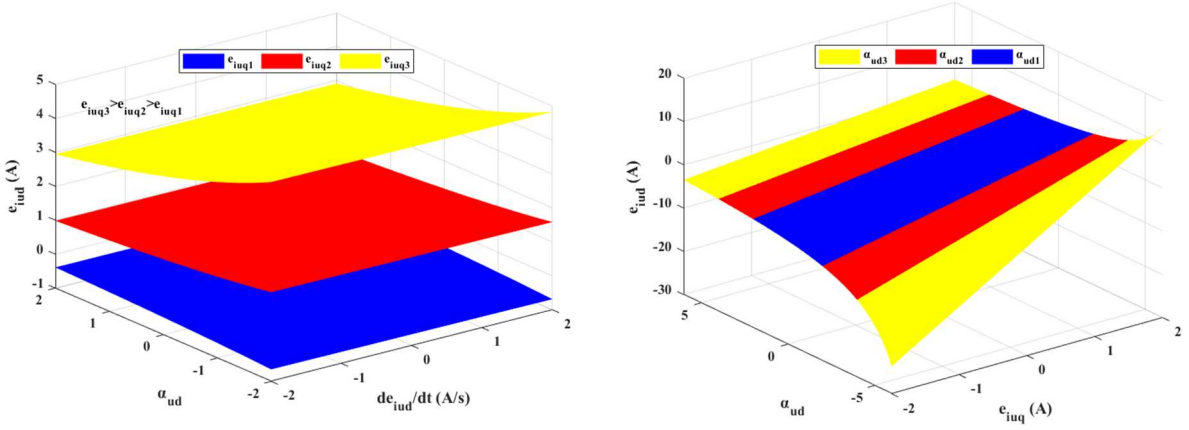

(a) (b)

Fig.3. The effects of Lypunov coefficients on the MMC state variable error and its dynamic, (a) when the error of e_{iuq} in increased, and (b) the interval of Lyapunov coefficients are extended.

V. The Separated Capability Curves for Upper and Lower Arms of MMCs

The d and q –components of MMCs upper and lower arms currents are able to generate a specific power. This point is considered in this paper to propose two separated capability

curves. These curves will demonstrate the power injection capability of MMCs upper and lower arms. To this end, the relation between the DC-link input power and terminal power is firstly stated as the follows,

$$v_{dc}i_{dc} = v_{td}i_d + v_{tq}i_q \tag{31}$$

It can be found from Fig. 1(b) that the d and q components of MMCs output currents are equalized to $i_d=i_{ud}-i_{ld}$ and $i_q=i_{uq}-i_{lq}$, respectively. Using the aforesaid relations, (31) is rewritten according to (32),

$$\frac{v_{dc}i_{dc}}{2R} = \underbrace{\left(v_{td}i_{ud} + v_{tq}i_{uq}\right)}_{Upper\ Arms} - \underbrace{\left(v_{td}i_{ld} + i_{lq}v_{tq}\right)}_{Lower\ Arms} \tag{32}$$

The terminal voltages v_{td} and v_{tq} can be stated based on the upper and lower arm state variables and parameters by applying KVL's law to Fig.1(b),

$$v_{td(q)} = \frac{v_{dc}}{2} - v_{ud(q)} - L_u\frac{di_{ud(q)}}{dt} - R_u i_{ud(q)} \pm \omega L_u i_{uq(\mathrm{d})} \tag{33}$$

$$v_{td(q)} = -\frac{v_{dc}}{2} + v_{ld(q)} + L_l\frac{di_{ld(q)}}{dt} + R_l i_{ld(q)} \mp \omega L_l i_{lq(\mathrm{d})} \tag{34}$$

By substituting the proposed modulation functions (11) into (33) and (34), the various terms of (32) are obtained as the following,

$$v_{td}i_{ud} = \frac{v_{dc}}{2}i_{ud} + 2L\frac{di_{ud}}{dt}i_{ud} + 2Ri_{ud}i_{ud} - 2\omega Li_{uq}i_{ud} + v_d i_{ud} \tag{35}$$

$$v_{tq}i_{uq} = \frac{v_{dc}}{2}i_{uq} + 2L\frac{di_{uq}}{dt}i_{uq} + 2Ri_{uq}i_{uq} + 2L\omega i_{ud}i_{uq} + v_q i_{uq} \tag{36}$$

$$v_{td}i_{ld} = -\frac{v_{dc}}{2}i_{ld} - 2L\frac{di_{ld}}{dt}i_{ld} - 2Ri_{ld}i_{ld} + 2L\omega i_{lq}i_{ld} + v_d i_{ld} \tag{37}$$

$$v_{tq}i_{lq} = -\frac{v_{dc}}{2}i_{lq} - 2L\frac{di_{lq}}{dt}i_{lq} - 2Ri_{lq}i_{lq} - 2L\omega i_{ld}i_{lq} + v_q i_{lq} \tag{38}$$

The power of MMCs upper and lower arms are firstly defined as $P_{ud(q)}=v_{dc}i_{ud(q)}$ and $P_{ld(q)}=v_{dc}i_{ld(q)}$. Then, by substituting the relations (35)-(38) into (31), two proposed capability curves are achieved as the following,

$$\left(P_{ud} + \underbrace{\left(\frac{v_{dc}^2}{8R} + \frac{Lv_{dc}}{2R}\frac{di_{ud}}{dt} + \frac{v_d v_{dc}}{4R}\right)}_{a_u}\right)^2 + \left(P_{uq} + \underbrace{\left(\frac{v_{dc}^2}{8R} + \frac{Lv_{dc}}{2R}\frac{di_{uq}}{dt} + \frac{v_q v_{dc}}{4R}\right)}_{b_u}\right)^2 = \underbrace{\left(\frac{v_{dc}^2}{8R} + \frac{Lv_{dc}}{2R}\frac{di_{ud}}{dt} + \frac{v_d v_{dc}}{4R}\right)^2 + \left(\frac{v_{dc}^2}{8R} + \frac{Lv_{dc}}{2R}\frac{di_{uq}}{dt} + \frac{v_q v_{dc}}{4R}\right)^2 + \frac{v_{dc}^3 i_{dc}}{4R}}_{r_u^2} \tag{39}$$

$$\left(P_{ld}+\underbrace{\left(\frac{v_{dc}^2}{8R}+\frac{Lv_{dc}}{2R}\frac{di_{ld}}{dt}-\frac{v_d v_{dc}}{4R}\right)}_{a_l}\right)^2+\left(P_{lq}+\underbrace{\left(\frac{v_{dc}^2}{8R}+\frac{Lv_{dc}}{2R}\frac{di_{lq}}{dt}-\frac{v_q v_{dc}}{4R}\right)}_{b_l}\right)^2= \tag{40}$$

$$\underbrace{\left(\frac{v_{dc}^2}{8R}+\frac{Lv_{dc}}{2R}\frac{di_{ld}}{dt}-\frac{v_d v_{dc}}{4R}\right)^2+\left(\frac{v_{dc}^2}{8R}+\frac{Lv_{dc}}{2R}\frac{di_{lq}}{dt}-\frac{v_q v_{dc}}{4R}\right)^2+\frac{v_{dc}^3 i_{dc}}{4R}}_{r_l^2}$$

Two proposed curves for upper and lower arms are drawn in Fig. 4(a). In this figure, the common area for power generation of both arms is specified. When the rated values of input and output voltages are increased, the curves are changed according to Fig. 4(b). In this condition, the common area of power generation is raised as well. On the other hand, when the input and output voltages of MMCs are increased, the ability of each arm at more power injection is noticeably enhanced as depicted in Fig. 4(b).

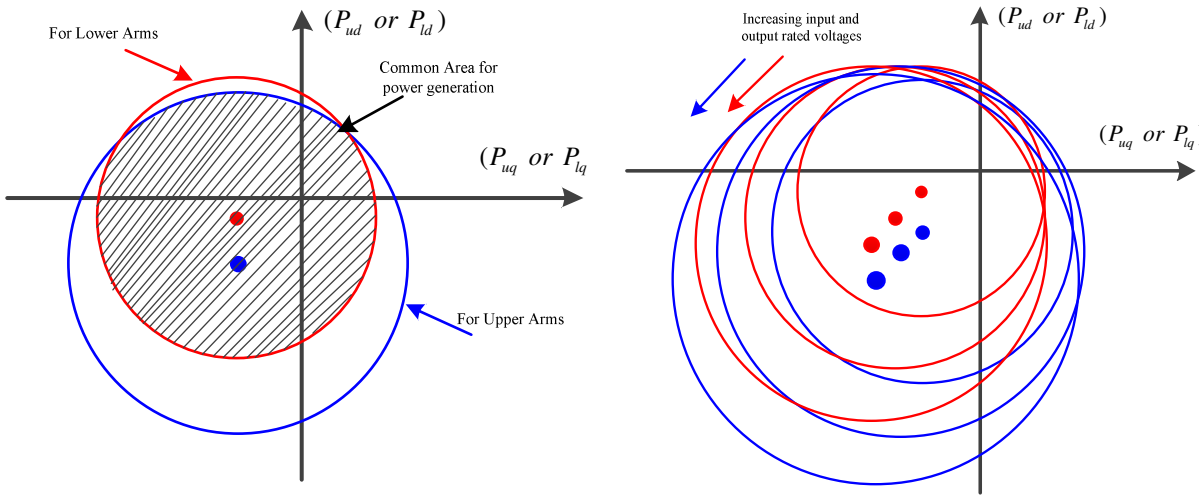

Fig.4. Proposed capability curves for upper and lower arms, (a) steady state condition, and (b) under increasing the input and output voltages of MMCs.

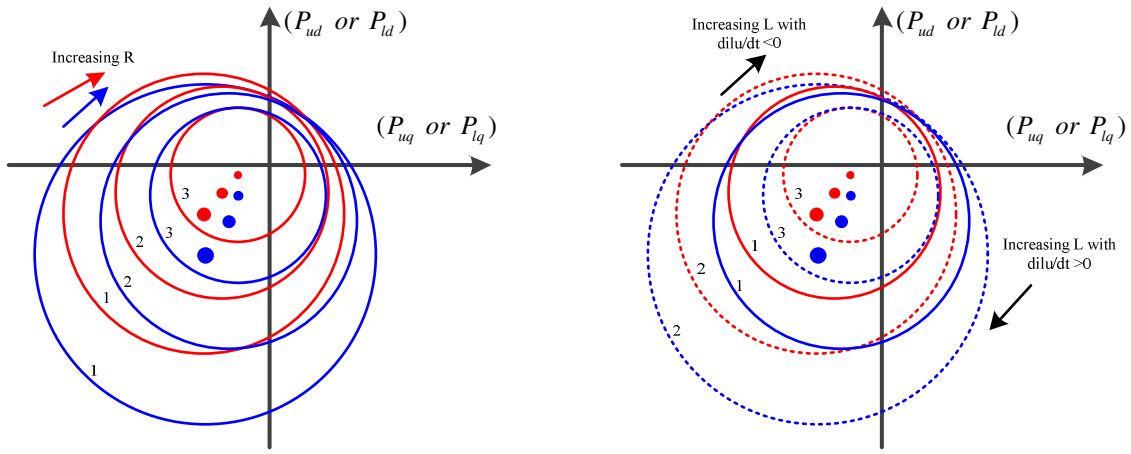

Fig.5. Proposed capability curves for upper and lower arms, (a) under increasing *R*, and (b) under increasing *L* with both negative and positive values for di_{lu}/dt.

Fig.5 shows the proposed capability curves under varying the MMC inductance and resistance. It can be observed from Fig. 5(a) that the increment of MMC resistance will lead to decreasing the area of the curves. It causes the common area of power generation to be mitigated. Consequently, less MMC resistance can enhance the ability of MMC's arms at generating more power. On the other hand, in the operating condition of $di_{lu}/dt<0$ with the increment of L, the capability curves of MMCs become smaller as shown in Fig. 5(b). In contrast, when the MMC inductance is increased with $di_{lu}/dt>0$, both capability curves for the MMCs upper and lower arms approach to bigger radius with significant increment at its center coordination.

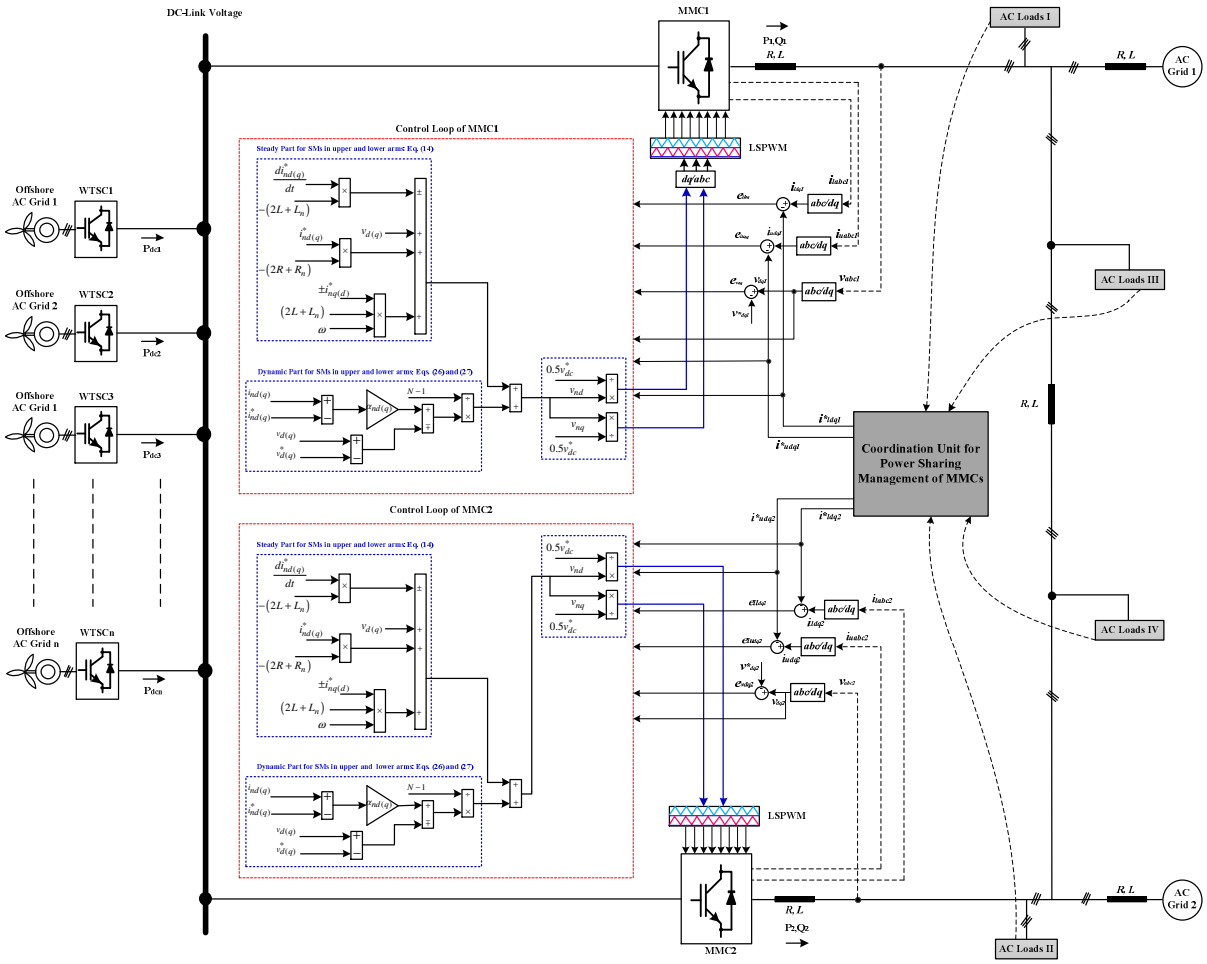

Fig.6. The overall structure of proposed control strategy for MT MMC-HVDC system.

TABLE I

SIMULATION PARAMETERS

MMCs SM Capacitor (C)	5 mF	DC-link Voltage	320 KV
MMCs Arm Inductance (L_b)	1 mH	AC Voltage	220 KV
MMCs Arm Resistance (R_b)	0.5 Ω	SMs Number/SMs Voltage	10/32 KV
MMCs Output Inductance (L_f)	5 mH	f_s (Switching Frequency)	2 kHz
MMCs Output Resistance (R_f)	0.1 Ω	f_{ac} (AC Voltage Frequency)	50 Hz

VI. Simulation Results

The MT MMC-HVDC system is simulated through MATLAB/Simulink, when the proposed control strategy is applied as depicted in Fig. 6. Both load and DC-link voltage variations exist in the MT MMC-HVDC system to validate the ability of proposed controller under dynamic operating conditions. Two AC grids 1 and 2 will be under load changes at t=15s and t=10s, respectively. The parameters of the considered MT MMC-HVDC system are given in Table I. The DC-link voltage is shown in Fig. 7. According to this figure, the

DC-link voltage is fluctuated with both steady-state and dynamic errors during the entire simulation time. In addition, as it can be seen from Fig. 6, a coordination unit is employed for MT MMC-HVDC system to provide a coordinated operation between MMC1 and MMC2 through the reference values archived for the related proposed control strategy.

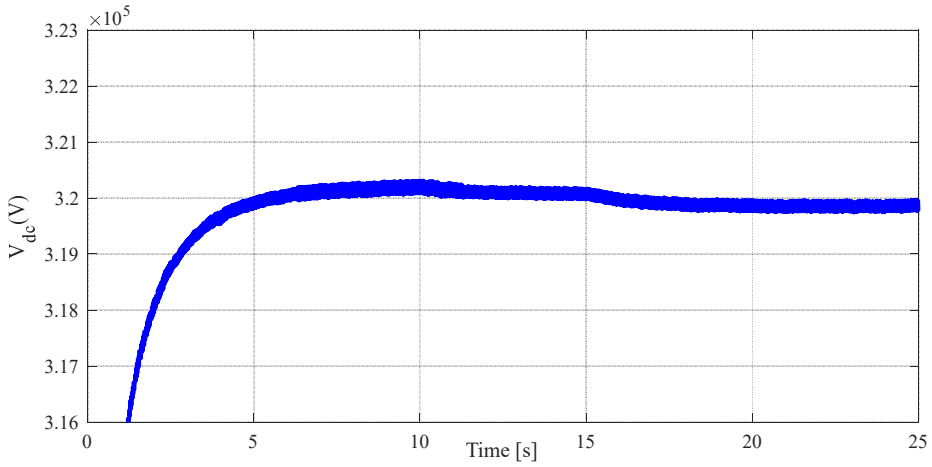

Fig.7. DC link voltage of the considered MT MMC-based HVDC system.

A. MMCs Operating Responses

In this sub-section, the performance of MMCs will be assessed when MMCs act in MT HVDC structure. Fig. 8 illustrates the active power of MMCs injected to both AC grids. It is obvious from this figure that both MMCs are able to track their reference values under load and DC-link voltage variations. However, compared to the operation of MMC2, MMC1 can provide a dynamic response with less overshoot. On the other hand, the reactive power of MMCs in AC grids are demonstrated in Fig.9. As it is predicted, appropriate steady and dynamic responses can be achieved for the reactive power of both MMCs during load and DC-link voltage as well. The reactive power injected to AC grid 1 has less undershoot compared to another reactive power response, as depicted in Fig.9. The SM capacitor voltages of both MMCs are demonstrated in Fig. 10 and Fig. 11. It can be understood from Figs. 10 and 11 that there is no special difference between the upper and lower SM capacitor voltages of MMC1 and MMC2. In addition, there is actable steady-state errors and negligible dynamic transients for both the upper and lower SM capacitor voltages under both load and DC-link voltage variations.

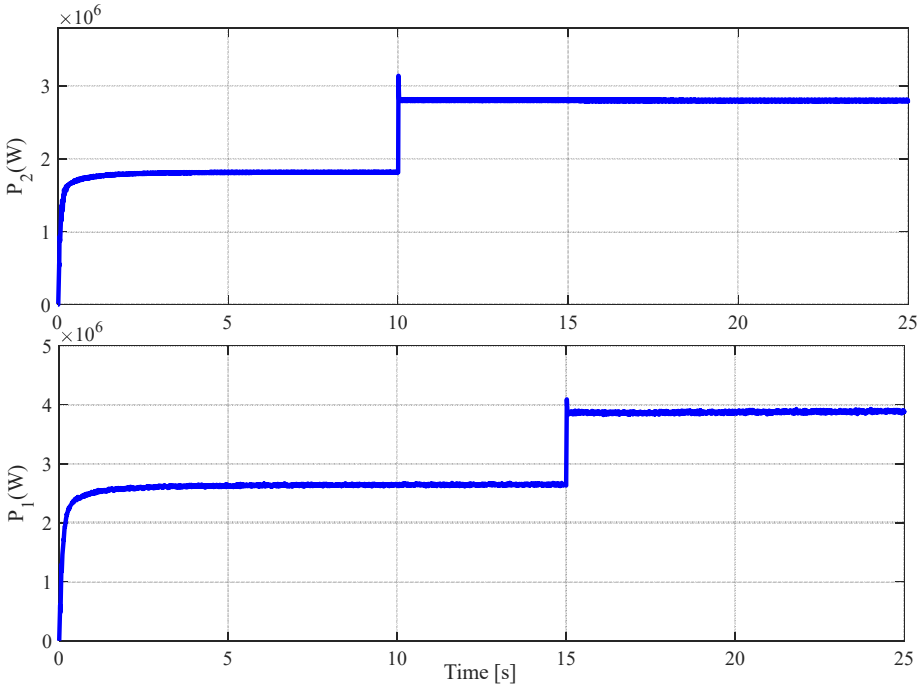

Fig.8. The active power injected to AC grids by MMCs.

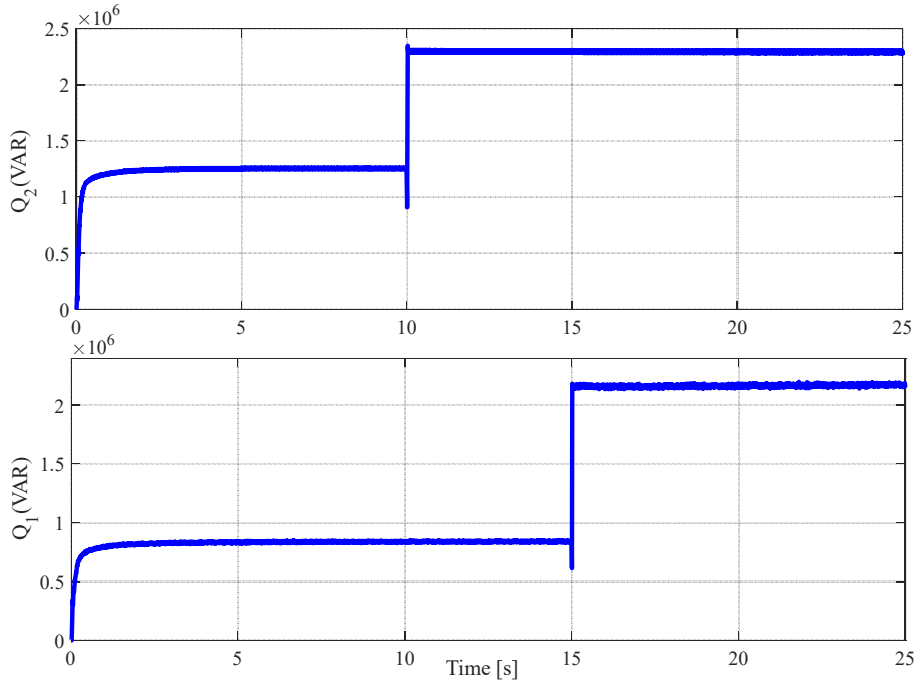

Fig.9. The reactive power injected to AC grids by MMCs.

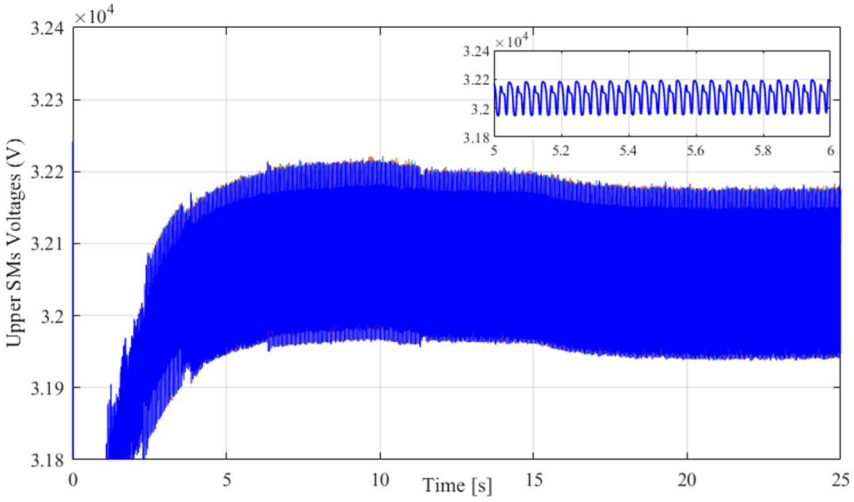

Fig.10. The upper SMs capacitor voltages of AC grids-MMCs.

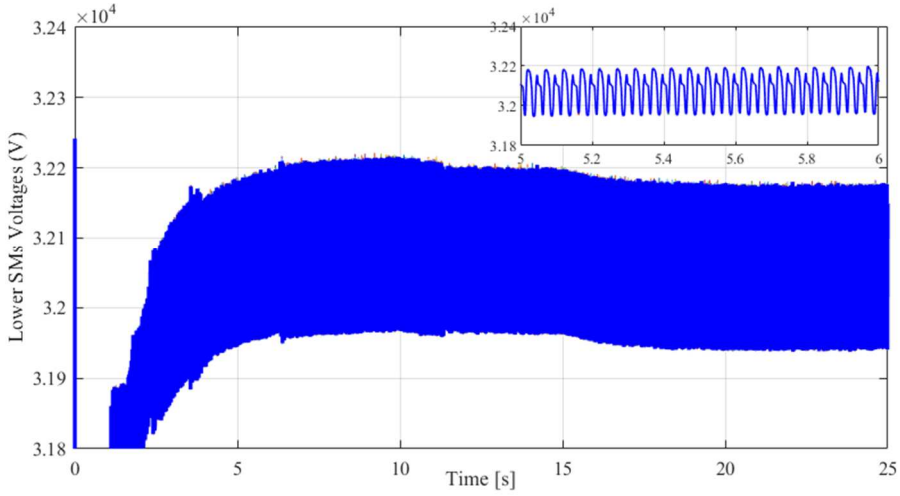

Fig.11. The lower SMs capacitor voltages of AC grids-MMCs.

B. Output Voltages of AC Sides

Frequency and voltage magnitude are two main specifications of output AC voltages of MMCs. The steady-state and dynamical responses of these specification will be evaluated in this sub-section when both DC-link voltage and loads are changed. The frequencies of voltages in AC grid 1 and 2 are demonstrated in Fig.12. The frequency response regarding AC grid 1 voltage is more fluctuated. However, according to Fig.12, the fluctuations are within an acceptable range under 0.4% error. In contrast, the frequency of AC grid 2 voltage has negligible steady-state and dynamic errors as shown in Fig. 12. Fig. 13 exhibits the magnitudes of AC grid voltages. Based on this figure, the voltage magnitude of AC grid 2 has steady state error less than 2% with insignificant oscillations. In comparison with AC grid 2, the dynamic response regarding the voltage magnitude of AC gird 1 has more undershoot. Also its steady state responses are involved with a little more fluctuation around 2% error as depicted in Fig. 13.

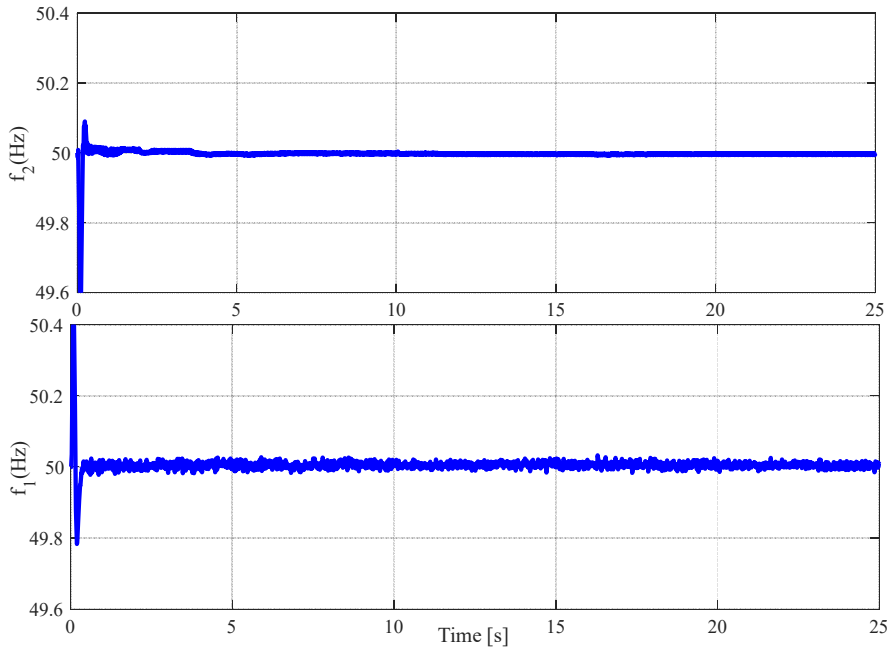

Fig.12. The Frequency responses of AC grids.

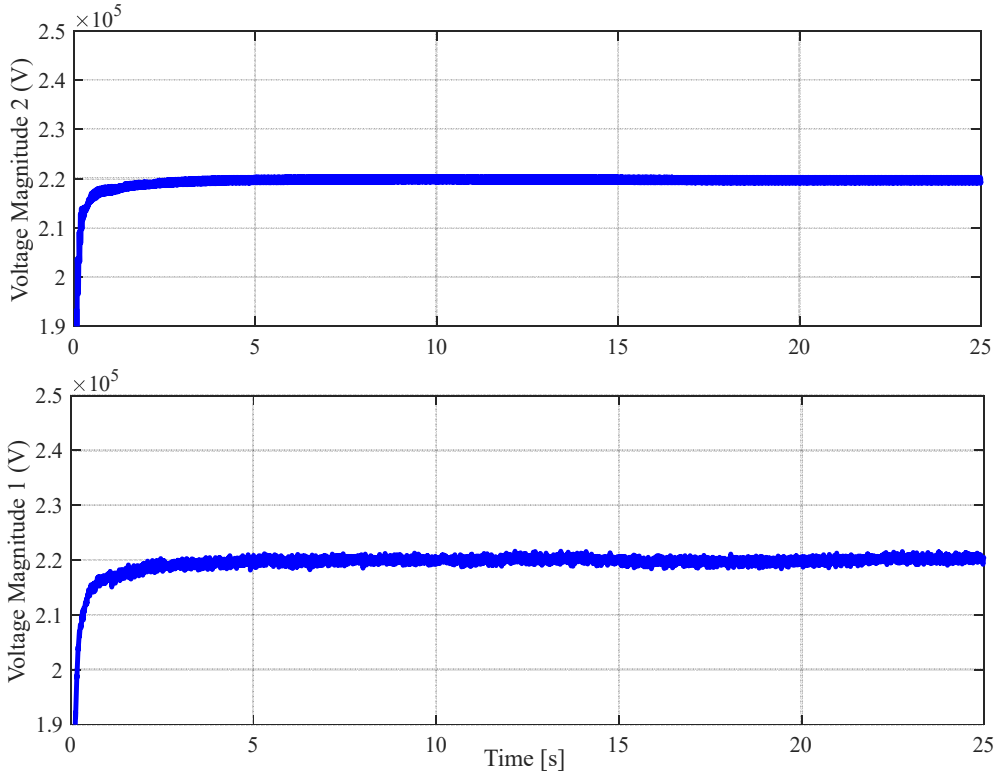

Fig.13. The voltage magnitude responses of AC grids.

VII. Conclusion

The stable operating conditions of a MT MMC-HVDC system have been provided in this paper through a new set of dynamic equations for MMCs and direct Lyapunov method. As the first contribution, a new dynamic model has been firstly achieved using the separated

state variables of MMC's upper and lower arms with high decoupling features. In the first step, these decoupling state variables have been set to make steady-state control functions with steady values of MMC arm's currents and output voltage in d-q reference frame. Then, stable dynamic parts have been achieved by Lyapunov energy function which guarantee very simple decoupled components for proposed control technique applied to MT MMC-HVDC system. Also, it has been completely contributed to finding out how the Lyapunov coefficients can impact on MMC errors and its dynamics. In order to more survey the effects of variations of MMC parameters and state variables, as another main contribution, two novel capability curves based on the power injection capability of MMC's upper and lower arms have been introduced as well. Using MATLAB/SIMULINK software, under variation of load and DC link voltage, it has been verified that accurate steady state and dynamic responses for MMCs active and reactive power sharing, SM's capacitors voltages, the voltage magnitude and frequency of output voltages could be obtained.

REFERENCES

[1] Sharifabadi K, Harnefors L, Nee H-P, Norrga St, Teodorescu R. Design, Control, and Application of Modular Multilevel Converters for HVDC Transmission Systems. John Wiley & Sons (2016); Book.

[2] Mehrasa M, Pouresmaeil E, Sepehr A, Pournazarian B, Catalão J P S. Control of Power Electronics-based Synchronous Generator for the Integration of Renewable Energies into the Power Grid. International Journal of Electrical Power & Energy Systems 2019; 111: 300-314.

[3] Staudt V, Jäger M K, Meyer D, Bartelt R, Heising C. Reaction of Grid-Connected Converters to Unbalanced Grid Voltages with Focus on Modular Multilevel Converters. International School on Nonsinusoidal Currents and Compensation (ISNCC), Lagow 2015; 1-5.

[4] Holari Y T, Taher S A, Mehrasa M. Distributed Energy Storage System-based Nonlinear Control Strategy for Hybrid microgrid Power Management Included Wind/PV Units in Grid-Connected Operation. International Transactions on Electrical Energy Systems 2020; 30 (2): e12237.

[5] Zama A, Bacha S, Benchaib A, Frey D, Silvant S. A Novel Modular Multilevel Converter Modelling Technique based on Semi-Analytical Models for HVDC Application" Journal of Electrical Systems 2016; 12(4): 649-659.

[6] Staudt V, Bartelt R, Heising C. Fault Scenarios in DC Ship Grids: The Advantages and Disadvantages of Modular Multilevel Converters. IEEE Electrification Magazine 2015; 3(2), 40-48.

[7] Babaie M, Sharifzadeh M, Mehrasa M, Chouinard G, Al-Haddad K. Supervised Learning Model Predictive Control Trained by ABC Algorithm for Common Mode Voltage Suppression in NPC Inverter. IEEE Journal of Emerging and Selected Topics in Power Electronics 2020; doi: 10.1109/JESTPE.2020.2984674.

[8] Alizadeh M, Kojori S S. Small-Signal Stability Analysis, and Predictive Control of Z-Source Matrix Converter Feeding a PMSG-WECS. International Journal of Electrical Power & Energy Systems 2018; 95: 601-616.

[9] Eimeni S N H, Radan A, Mehrasa M. The Single-Phase Single-Switch PWM Three-Level High Power Factor Rectifier for DC Network Application. 4th IEEE Conference on Industrial Electronics and Applications, Xi'an 2009; 1419-1424.

[10] Harnefors L, Johansson N, Zhang L. Impact on Interarea Modes of Fast HVDC Primary Frequency Control. IEEE Transactions on Power Systems 2017; 32(2): 1350-1358.

[11] Sharifzadeh M, Mehrasa M, Babaie M, Al-Haddad K. Stable Frequency Response for Multi-Terminal MMC-HVDC System with DC Voltage Fluctuations. 45th Annual Conference of the IEEE Industrial Electronics Society 2019; 3577-3582.

[12] Hu P, Guerrero J M, He Z. Design and Analysis of a Transformerless STATCOM based on Hybrid Cascaded Multilevel Converter. International Journal of Electrical Power & Energy Systems 2019; 104: 694-704.

[13] Pires V F, Fialho J, Silva J F. HVDC Transmission System using Multilevel Power Converters based on Dual Three-Phase Two-Level Inverters. International Journal of Electrical Power & Energy Systems 2015; 65: 191-200.

[14] Babaie M, Sharifzadeh M, Mehrasa M, Chouinard G, Al-Haddad K. PV Panels Maximum Power Point Tracking based on ANN in Three-Phase Packed E-Cell Inverter. IEEE International Conference on Industrial Technology (ICIT) 2020; 854-859.

[15] Harnefors L, Antonopoulos A, Norrga S, Angquist L, Nee H. Dynamic Analysis of Modular Multilevel Converters. IEEE Transactions on Industrial Electronics 2013; 60(7): 2526-2537.

[16] Bessegato L, Harnefors L, Ilves K, Norrga S. A Method for the Calculation of the AC-Side Admittance of a Modular Multilevel Converter. IEEE Transactions on Power Electronics 2019; 34(5): 4161-4172.

[17] Mehrasa M, Pouresmaeil E, Zabihi S, Caballero J C T, Catalão J P S. A Novel Modulation Function-based Control of Modular Multilevel Converters for High Voltage Direct Current Transmission Systems. Energies 2016; 9(11): 867.

[18] Ilves K, Taffner F, Norrga S, Antonopoulos A, Harnefors L, Nee H. A Submodule Implementation for Parallel Connection of Capacitors in Modular Multilevel Converters. IEEE Transactions on Power Electronics 2015; 30(7): 3518-3527.

[19] Mehrasa M, Godina R, Pouresmaeil E, Rodrigues E M G, Catalão J P S. Power Quality Improvement with a Pulse Width Modulation Control Method in Modular Multilevel Converters under Varying Nonlinear Loads. Applied Sciences 2020; 10(9): 3292.

[20] Bessegato L, Norrga S, Ilves K, Harnefors L. Ac-Side Admittance Calculation for Modular Multilevel Converters. 3rd International Future Energy Electronics Conference and ECCE Asia (IFEEC 2017 - ECCE Asia 2017; 308-312.

[21] Lesnicar A, Marquardt R. An Innovative Modular Multilevel Converter Topology Suitable for a Wide Power Range. In Proc. IEEE Bologna Power Tech 2003; 3.

[22] Hagiwara M, Nishimura K, Akagi H. A Medium-Voltage Motor Drive with a Modular Multilevel PWM Inverter. IEEE Trans. Power Electron 2010; 25(7): 1786–1799.

[23] Mehrasa M, Pouresmaeil E, Zabihi S, Vechiu I, Catalão J P S. A Multi-Loop Control Technique for the Stable Operation of Modular Multilevel Converters in HVDC Transmission Systems. International Journal of Electrical Power & Energy Systems 2018; 96: 194-207.

[24] Duarte S N, Almeida P M.de, Barbosa P G. A Novel Energizing Strategy for a Grid-Connected Modular Multilevel Converter Operating as Static Synchronous Compensator. International Journal of Electrical Power & Energy Systems 2019; 109: 672-684.

[25] Li H, Xie X, McDonald A, Chai Z, Yang T, Wu Y, Yang W. Cost and Reliability Optimization of Modular Multilevel Converter with Hybrid Submodule for Offshore DC Wind Turbine. International Journal of Electrical Power & Energy Systems 2020; 120: 105994.

[26] Páez J D, Frey D, Maneiro J, Bacha S, Dworakowski P. Overview of DC–DC Converters Dedicated to HVdc Grids. IEEE Transactions on Power Delivery 2019; 34(1): 119-128.

[27] Jäger M K, Staudt V, Steimel A, Meyer D, Heising C. Power-Transmission via an MMC-based HVDC System for the Rededication of Existing AC-Lines. In: Schulz D. (eds) NEIS Conference (Springer) 2016; 32-38.

[28] Mehrasa M. Control of Modular Multilevel Converters in High Voltage Direct Current Power Systems. PhD Thesis, June 2019.

[29] Mehrasa M, Pouresmaeil E, Taheri S, Vechiu I, Catalão J. P. S. Novel Control Strategy for Modular Multilevel Converters based on Differential Flatness Theory. IEEE Journal of Emerging and Selected Topics in Power Electronics 2018; 6(2): 888-897.

[30] Mehrasa M, Pouresmaeil E, Akorede M F, Zabihi S, Catalão J P S. Function-based Modulation Control for Modular Multilevel Converters under Varying Loading and Parameters Conditions. IET Generation, Transmission & Distribution 2017; 11(13): 3222-3230.

[31] Stoetzel T, Jäger M K, Heising C, Staudt V. Analysis of DC-Droop Control for an MMC-based HVDC System. Mediterranean Conference on Power Generation, Transmission, Distribution and Energy Conversion 2016; 1-7.

[32] Ramirez D, Zarei M E, Gupta M, Serrano J. Fast Model-based Predictive Control (FMPC) for Grid Connected Modular Multilevel Converters (MMC). International Journal of Electrical Power & Energy Systems 2020; 119: 105951.

[33] Belhaouane M M, Ayari M, Guillaud X, Braiek N B. Robust Control Design of MMC-HVDC Systems Using Multivariable Optimal Guaranteed Cost Approach. IEEE Transactions on Industry Applications 2019; 55(3): 2952-2963.

[34] F. Yan et al. Coordinated Start-Up Control and Inter-Converter Oscillations Damping for MMC-HVDC Grid. IEEE Access 2019; 7: 65093-65102.

[35] Beheshti N, Rezanejad M, Mehrasa M. Linearized Control Technique with Lyapunov Function-based Compensators for MMC-based HVDC System under Load Variation and Fault Condition. International Journal of Electrical Power & Energy Systems 2021; 124: 106333.

[36] Jäger M K, Staudt V, Steimel A, Meyer D, Heising C. Power-Transmission of a MMC-based Multiterminal HVDC System in Monoplar Configuration. Mediterranean Conference on Power Generation, Transmission, Distribution and Energy Conversion 2016; 1-6.

[37] Liang J, Gomis-Bellmunt O, Ekanayake J, Jenkins N, An W. A Multi-Terminal HVDC Transmission System for Offshore Wind Farms with Induction Generators. International Journal of Electrical Power & Energy Systems 2012; 43(1): 54-62.

[38] Jahn I, Hohn F, Chaffey G, Norrga S. An Open-Source Protection IED for Research and Education in Multiterminal HVDC Grids. IEEE Transactions on Power Systems 2020; 35(4): 2949-2958.

[39] Zhao H, Lin Z, Wu Q, Huang S. Model Predictive Control based Coordinated Control of Multi-Terminal HVDC for Enhanced Frequency Oscillation Damping. International Journal of Electrical Power & Energy Systems 2020; 123: 106328.

[40] Deng N, Wang P, Zhang X-P, Tang G, Cao J. A DC Current Flow Controller for Meshed Modular Multilevel Converter Multiterminal HVDC Grids. CSEE Journal of Power and Energy Systems 2015; 1(1): 43–51.

[41] Abdel-Khalik A. S, Massoud A. M, Elserougi A. A, Ahmed S. Optimum Power Transmission-Based Droop Control Design for Multi-Terminal HVDC of Offshore Wind Farms. IEEE Transactions on Power Systems 2013; 28(3): 3401–3409.

[42] Chen J, Li L, Dong F, Wang X, Sheng H, Sun C, Li G. An Improved Coordination Method of Multi-Terminal MMC-HVDC System Suitable for Wind Farm Clusters Integration," International Journal of Electrical Power & Energy Systems 2020; 117: 105652.

[43] Givaki K, Rahman M. H, Vozikis D, Giveki A. Analysis of Integration of Multi-Terminal HVDC Network to Weak Grids. The Journal of Engineering 2019; 16: 3219–3224.

[44] Freytes J, Akkari S, Rault P, Belhaouane M. M, Gruson F, Colas F, Guillaud X. Dynamic Analysis of MMC-Based MTDC Grids: Use of MMC Energy to Improve Voltage Behavior. IEEE Transactions on Power Delivery 2019; 34(1): 137–148.

[45] Bernal-Perez S, Añó-Villalba S, Blasco-Gimenez R. Stability Analysis of Multi-Terminal HVDC with Diode Rectifier Connected Off-Shore Wind Power Plants. International Journal of Electrical Power & Energy Systems 2021; 124: 106231.

[46] Ahmed N, Ängquist L, Mahmood S, Antonopoulos A, Harnefors L, Norrga S, Nee H-P. Efficient Modeling of an MMC-Based Multiterminal DC System Employing Hybrid HVDC Breakers. IEEE Transactions on Power Delivery 2015; 30(4): 1792-1801.

[47] Lin N, Dinavahi V. Dynamic Electro-Magnetic-Thermal Modeling of MMC-Based DC–DC Converter for Real-Time Simulation of MTDC Grid. IEEE Transactions on Power Delivery 2018; 33(3): 1337–1347.

[48] Mehrasa M, Ahmadigorji M, Abedi A. Dual Lagrangian modeling and Lyapunov-based Control of Three-Level Three-Phase NPC Voltage-Source Rectifier. 11th International Conference on Environment and Electrical Engineering 2012; 737-743.

[49] Mehrasa M, Ahmadigorji M, Amjady N. A New Dual Lagrangian Model and Input/Output Feedback Linearization Control of 3-Phase/Level NPC Voltage-Source Rectifier. Automatika 2014; 55 (1): 99-111.

[50] Tang G, Xu Z, Dong H, Xu Q. Sliding Mode Robust Control Based Active-Power Modulation of Multi-Terminal HVDC Transmissions. IEEE Transactions on Power Systems 2016; 31(2): 1614–1623.

[51] Bergna-Diaz G, Zonetti D, Sanchez S, Ortega R, Tedeschi E. PI Passivity-Based Control and Performance Analysis of MMC Multiterminal HVDC Systems. IEEE Journal of Emerging and Selected Topics in Power Electronics 2019; 7(4): 2453-2466.

[52] Mehrasa M, Lesan S, Emeni S N H, Sheikholeslami A. Passivity-based Control with Dual Lagrangian Model of Four-Wire Three-Level Three-Phase NPC Voltage-Source Rectifier. Compatibility and Power Electronics 2009; 411-418.

[53] Ahmadijokani M, Mehrasa M, Sleiman M, Sharifzadeh M, Sheikholeslami A, Al-Haddad K. A Back-Stepping Control Method for Modular Multilevel Converters. IEEE Transactions on Industrial Electronics, doi: 10.1109/TIE.2019.2962455.

Annex A

The extended terms of (6) and (7):

$$\begin{cases} \left(2L+L_u\right)\dfrac{di_{ua}}{dt}+\left(2R+R_u\right)i_{ua}+v_{ua}+v_a=0 \\ \left(2L+L_u\right)\dfrac{di_{ub}}{dt}+\left(2R+R_u\right)i_{ub}+v_{ub}+v_b=0 \\ \left(2L+L_u\right)\dfrac{di_{uc}}{dt}+\left(2R+R_u\right)i_{uc}+v_{uc}+v_c=0 \end{cases} \tag{A-1}$$

$$\begin{cases} \left(2L+L_l\right)\dfrac{di_{la}}{dt}+\left(2R+R_l\right)i_{la}+v_{la}-v_a=0 \\ \left(2L+L_l\right)\dfrac{di_{lb}}{dt}+\left(2R+R_l\right)i_{lb}+v_{lb}-v_b=0 \\ \left(2L+L_l\right)\dfrac{di_{lc}}{dt}+\left(2R+R_l\right)i_{lc}+v_{lc}-v_c=0 \end{cases} \tag{A-2}$$

Annex B

The Park Transformation Matrix:

$$\begin{bmatrix} x_d \\ x_q \\ x_0 \end{bmatrix} = \frac{2}{3} \begin{bmatrix} \cos(\theta) & \cos\left(\theta - \frac{2\pi}{3}\right) & \cos\left(\theta + \frac{2\pi}{3}\right) \\ \sin(\theta) & \sin\left(\theta - \frac{2\pi}{3}\right) & \sin\left(\theta + \frac{2\pi}{3}\right) \\ \frac{1}{2} & \frac{1}{2} & \frac{1}{2} \end{bmatrix} \begin{bmatrix} x_a \\ x_b \\ x_c \end{bmatrix} \quad \text{(B-1)}$$